

SIMULATING STRONG GROUND MOTION FROM COMPLEX SOURCES BY RECIPROCAL GREEN FUNCTIONS

L. EISNER*, R.W. CLAYTON

Seismological Laboratory, 1200 California Blvd. 252-21, California Institute of Technology, Pasadena, CA91125, U.S.A.

* Presently at Schlumberger Cambridge Research Center, High Cross, Madingley Rd., Cambridge, CB12PR, U.K. (leisner@cambridge.oilfield.slb.com)

Received: April 22, 2003; Revised: January 15, 2005; Accepted: April 19, 2005

ABSTRACT

We have developed a method to calculate site and path effects for complex heterogeneous media using synthetic Green's functions. The Green's functions are calculated numerically by imposing body forces at the site of interest and then storing the reciprocal Green's functions along arbitrary finite-fault surfaces. By using reciprocal Green's functions, we can then simulate many source scenarios for those faults because the primary numerical calculations need be done only once. The advantage of the proposed method is shown by evaluation of the site and path effects for three sites in the vicinity of the Los Angeles basin using the Southern California Velocity Model (version 2.2, Magistrale et al., 2000). In this example, we have simulated 300 source scenarios for 5 major southern California faults and compared their responses for period longer than 3 seconds at the selected sites. However, a more detailed comparison with strong motion records will be necessary before a particular hazard assessment can be made. For the tested source scenarios the results show that the variations in the peak velocity amplitudes and durations due to a source scenarios are as large as variations due to a heterogeneous velocity model.

Keywords: full waveform modeling, seismic hazard, finite source, rupture propagation, hazard assessment, finite difference, Los Angeles Basin

1. INTRODUCTION

A significant effort has been devoted to include synthetic simulations and observed data into the evaluation of the site and path effects in seismic hazard analyses (c.f. *Field et al., 2000*). Recently numerical simulations of long-period strong ground motion in heterogeneous media were shown to be capable of reproducing the characteristic parameters of the observed data (*Olsen and Archuleta, 1996; Wald and Graves, 1998; Eisner and Clayton, 2002a*). Our goal is to include these long-period simulations into seismic hazard analyses as they have the potential to predict the strong ground motions more accurately than empirical relationships based on strong motion observations not directly related to a particular site.

The method currently used for the calculation of site and path effects by full waveform modeling has been developed by *Olsen and Archuleta (1996)*. They account for site and path effects by evolving the wavefield outward from the source location to a suite of sites, which means that one complete simulation is needed for each source location and scenario. However, it has been pointed out (*Field et al., 2000*) and we will show in this study, that site and path effects depend significantly on the particular choice of source location and scenario. Therefore, to estimate seismic hazard more accurately we need to simulate a large number of source locations and realistic scenarios. The reciprocity method (*Liu and Archuleta, 2000; Eisner and Clayton, 2001; Graves and Wald, 2001*) allows us to simulate a large number of source scenarios without re-calculating the Green's functions. In this way, the problem is divided into a component that is independent of the rupture scenario and one that depends on it. This method does require three numerical simulations of the wavefield for each site (*Eisner and Clayton, 2001*). The reciprocity method and Southern California model were calibrated in a previous study (*Eisner and Clayton, 2002a*) by comparison of a large number of weak-motion earthquake recordings with synthetic seismograms. The strong-motion seismograms are evaluated by superposition of time-staggered point sources. The technique of superposition of point sources was used and validated for southern California by numerous studies, e.g. *Olsen and Archuleta (1996)*, *Wald and Graves (1998)*, or *Olsen (2000)*. In this study, we present a method for including a detailed rupture model and the wave propagation effects for strong motion studies, but the models will need to be calibrated with actual strong motion records before a particular hazard assessment can be made.

We apply this method to three selected sites in the Los Angeles basin: a site above the deep part of the basin, a site at the edge of the basin, and a hard rock site near the basin. For each site, we compute the effects of 300 hypothetical rupture scenarios on five major faults in the southern California, including the San Andreas fault. Therefore, we have reduced the number of numerical simulations by a factor of 33 (300/9).

2. METHOD, MODEL AND SOURCE PARAMETERIZATION

We compute site and path effects by imposing three orthogonal body forces at the site of interest and evaluating reciprocal Green's functions along the fault surfaces. We store the evaluated reciprocal Green's functions on the selected fault planes to simulate an arbitrary rupture scenario. We need the S-wave velocity and the rigidity modulus μ at the fault location to evaluate the rupture velocity and to scale the displacement on a particular segment of the fault. We have numerically found that we need to calculate the Green's functions at a minimum of three points per S-wave wavelength, to model an arbitrary source rupture scenario (in agreement with *Spudich, 1981*). The wavelength in this case, is that of the shortest S-wave traveling along the fault surface. To determine the rupture front history, we use the finite-difference travel-time method (*Vidale, 1988*) with velocities specified as a proportional fraction of the S-wave velocities along the fault surface as given in the model.

We used the values of rigidity modulus μ_n to scale the displacement on a fault segment to the seismic moment of that segment. A segment of area A_n and slip D_n has a seismic moment of

$$M_n = D_n A_n \mu_n .$$

This moment can be directly implemented for representation by a double-couple point-source in the finite-difference method (Graves, 1996). The total long-period moment M_0 is then given by the scalar sum

$$M_0 = \sum_{n=0}^K D_n A_n \mu_n , \quad (1)$$

where K is number of segments on the fault.

To relate the area S of the entire fault to the moment magnitude, we can use the empirical relationship derived from a global data set by Wells and Coppersmith (1994):

$$M_0 = 3.98 + 1.02 \log(S) . \quad (2)$$

Here M_0 is the total long-period moment measured in dyne-cm, S is the area of the entire fault in kilometers squared.

For a given M_0 , we can evaluate the rupture area S from Eq.(2). We then divide this area S into fault segments A_n , each with slip D_n , with the constraint imposed by Eq.(1). For a uniform slip D_u and the fault area S divided into equal area segments A , we have

$$D_u = \frac{M_0}{AK\bar{\mu}} = \frac{M_0}{S\bar{\mu}} , \quad (3)$$

where $\bar{\mu}$ is an arithmetic average of the rigidity modulus over the fault, and the n^{th} segment of the fault has a moment of

$$M_n = \frac{M_0}{AK\bar{\mu}} A \mu_n = \frac{M_0}{K} \frac{\mu_n}{\bar{\mu}} = \frac{M_0 \mu_n A}{S \bar{\mu}} . \quad (4)$$

The synthetic Green's functions were evaluated with the finite-difference method (Graves, 1996) for the Southern California Velocity Model Version 2.2 (Magistrale et al., 2000). This model of the southern California velocity structure includes the sedimentary basins, a laterally varying velocity structure outside of the basins, and a geotechnical layer of slow velocities near surface. We assume for the purposes of this paper that the three dimensional (3D) velocity model is correct, and do not consider the effects of errors in the model on the results. Olsen and Archuleta (1996) and Wald and Graves (1998) compared strong ground motion records from two large earthquakes in the vicinity of the Los Angeles basin. They have observed a good fit (within a factor of 2) between the maximum velocity amplitude of synthetic and recorded long period seismograms. Furthermore, the limitations of the Southern California velocity model are further tested in a previous study (Eisner and Clayton, 2002a) by comparison of a large number of weak motion records. Eisner and Clayton (2002a) show that the misfit between the maximum amplitude of data and synthetics has a significant variation with azimuth, but the model does not generate a systematic bias. In general, however, one may need to extend the simulations to include the uncertainty of the velocity model.

The attenuation effects on synthetic seismograms can be included as part of this method, if an attenuation model is available. In the case of Southern California Velocity Model Version 2.2 (Magistrale et al., 2000) attenuation is not available. In Appendix A,

we show estimates that indicate that attenuation could reduce the amplitudes at most by a factor of 2 for the period band selected in this study. We have not included that effect in the calculations in this study, because the attenuation model is not available and the effects of attenuation do not significantly affect our conclusions.

This study directly includes the top of the velocity layers with the low velocities as given in the Southern California Velocity Model. We have used the equivalent medium parameters method of *Eisner and Clayton (2002b)* to resample the top low velocity layers to avoid artifacts due to an arbitrary velocity clamping (establishing a floor on velocity values in the model). This finite difference model representation ensures that the original Southern California Velocity Model is properly represented for the wave propagation at long periods (greater than three seconds in this study). The sampling shown in *Eisner and Clayton (2002b)* accounts for both the site effects and propagation effects. The minimum velocity in the resampled model used for the numerical simulations was 0.5 km/s for modeling of a signal with periods of 3 seconds and longer. Love wave velocities are shown in Fig. 1. Love waves velocities show a combined effect of shear velocity and structure and are diagnostic of the focusing and amplification that will be produced by the model.

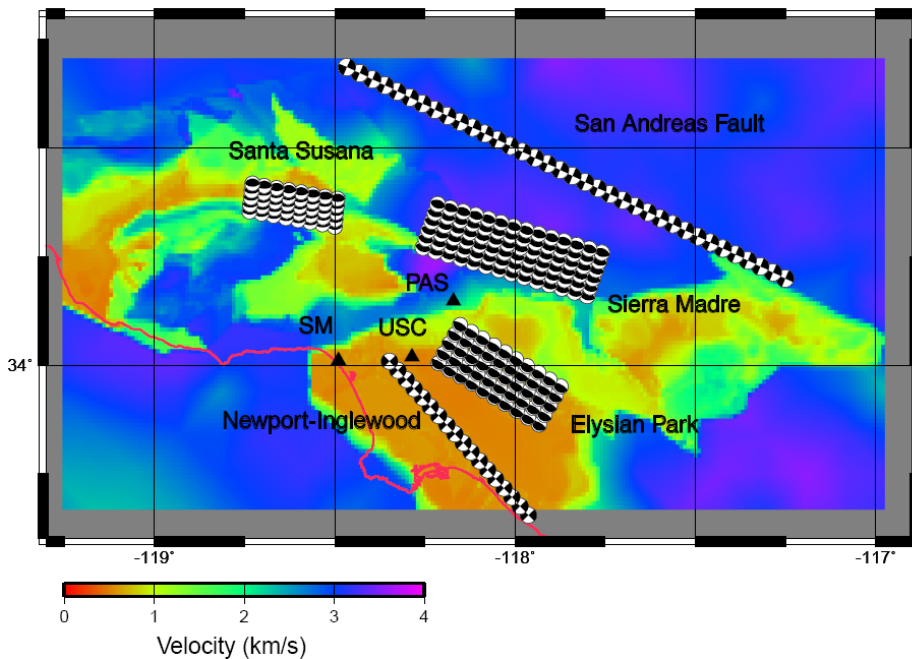


Fig. 1. Southern California Velocity Model and locations of the selected sites and faults. The velocity is the Love wave group velocity at 3 second period. The fault locations are shown with focal mechanisms as projected on the surface. Selected sites are shown with black triangles and capital letters: **PAS** - Pasadena, **USC** - University of Southern California, and **SM** - Santa Monica. The large low velocity area between -118.5° and -117.75° longitude and below 34.1° latitude is the Los Angeles Basin.

Table 1. List of the selected sites and their locations.

Site	Setting	Latitude [°N]	Longitude [°E]
SM	basin edge	34.011	-118.490
USC	deep basin	34.019	-118.286
PAS	hard rock	34.148	-118.171

Table 2. List of the selected faults and their parameters.

Fault Name	SE	NW	Dip	Rake	Strike
San Andreas	34.20-117.25	34.70-118.50	90	180	113
Newport-Inglewood	33.65-117.96	34.03-118.37	90	180	136
Santa Susana	34.32-118.50	34.44-118.76	55	90	91
Sierra Madre	34.16-117.80	34.40-118.24	45	90	107
Elysian Park	33.86-117.95	34.13-118.16	20	90	120

Fault Name	Length	Depth 1	Depth 2	M_w	D
San Andreas	120.0	0.0	18.0	7.4	2.0
Newport-Inglewood	60.0	0.0	13.0	6.9	1.3
Santa Susana	25.0	0.0	13.0	6.6	1.1
Sierra Madre	47.0	0.0	15.0	7.0	1.2
Elysian Park	33.0	10.0	15.0	6.7	1.2

To illustrate the reciprocity method applied to site effect evaluation, we have selected 3 sites and 5 major faults in southern California. The sites were chosen to demonstrate the strong ground motion responses at different locations relative to the Los Angeles Basin. Table 1 has a list of the sites with their locations. They are also shown in Fig. 1. Table 2 has a list of the basic parameters describing the faults. The fault parameters were taken from *Petersen et al. (1996)*.

To simulate the effects of dynamic rupture, we need to specify for each fault the slip distribution, rupture velocity, hypocenter, and time history of each point. For the purposes of this paper, we will consider distribution of these parameters, thus avoiding the issue of a preferred source scenario. However to produce a realistic analysis of seismic hazard, the parameters should probably be more finely and uniformly sampled. The main focus of this study is to introduce reciprocity method for evaluation of the site and path effects, therefore we include the detail description of the tested slip distribution, rupture velocity, hypocenter, and time history of each point in the Appendix B. However we would like to emphasize that the source parameters of the future earthquakes can be only estimated and it is up to the reader to consider if our estimate is sufficient. Where necessary we discuss possible effects various other source distributions on our conclusions.

Generally this method enables us to reduce the amount of full waveform calculation by a factor:

$$\frac{3 * ST}{F * SC} = \frac{3 * ST}{F * RVS * HL * SD * RT} \quad (5)$$

where ST is the number of sites, F is the number of faults, SC is the number of scenarios, RVS is the number of rupture velocity scenarios, HL is the number of hypocenter locations, SD is the number of slip distributions, and RT is the number of time histories of each point. We can clearly see that if the number of sites of interests is relatively small, this method results in a significant reduction in the required number of numerical simulations.

3. SITE AND PATH EFFECTS AT THE SELECTED SITES

We have calculated strong motion seismograms for periods longer than 3 seconds due to 300 fault rupture scenarios at the three sites. First we shall show examples of synthetic seismograms computed at the selected sites. Then we shall compare statistical properties of characteristics of the computed seismograms and analyze the observed results.

Fig. 2 shows the strong motion velocity seismograms with the largest recorded peak ground velocity amplitude of all of the modeled seismograms. The largest peak ground

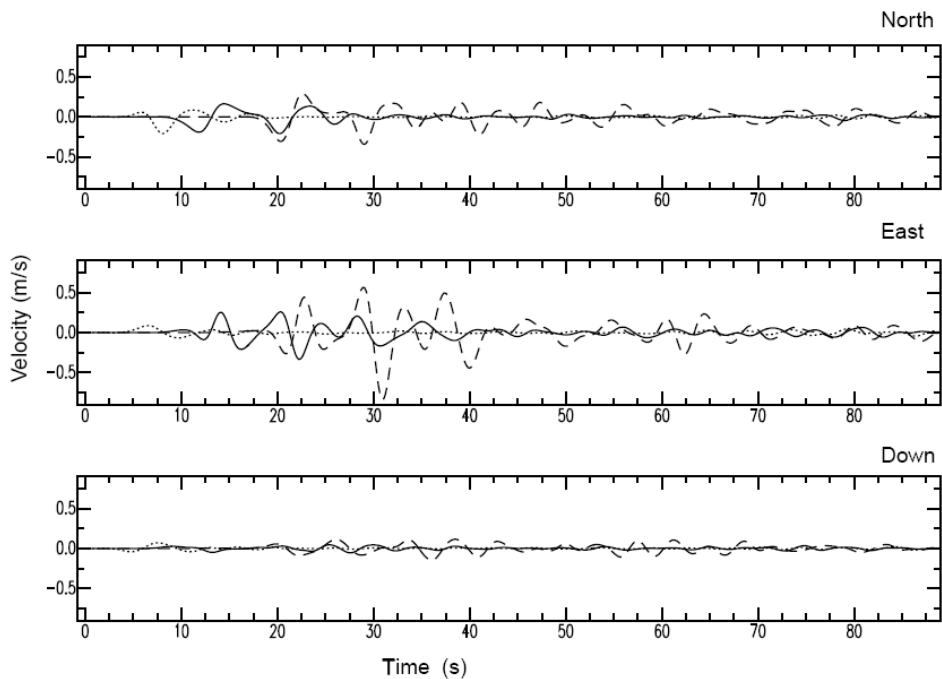


Fig. 2. Synthetic seismograms at the USC site with the scenario causing the largest recorded peak ground velocity amplitude in our simulations due to a rupture on the Newport-Inglewood fault with its hypocenter at the south-east edge at depth 6.5 km. The dotted line represents seismograms due to an earthquake with rupture velocity equal to 60% of the S-wave velocity, the solid line represents seismograms due to an earthquake with rupture velocity equal to 75% of S-wave velocity, and the dashed line represents seismograms due to an earthquake with rupture velocity equal to 90% of the S-wave velocity.

velocity amplitude was recorded at the closest site to a rupturing fault (USC site from the Newport-Inglewood fault) and for the fastest rupture velocity directed towards the site. Fig. 2 shows effects of the rupture velocity (and rupture directivity) on the synthetic seismograms. Generally, earthquakes with larger rupture velocities towards the observer produce larger ground motion levels at the observer's site (rupture directivity). However, the strong heterogeneity of the velocity on the fault makes the directivity effect less efficient as different parts of the fault propagate at different velocities and in different directions. The synthetic seismograms at the USC site are further complicated by the long duration of the coda following the initial peak as the energy released by the earthquake remains trapped in the Los Angeles basin.

Fig. 3 shows the synthetic seismograms at the USC site for the hypothetical earthquakes on the Newport-Inglewood fault with three hypocenter locations. It shows the effects of the hypocenter location and rupture directivity on the synthetic seismograms for the same rupture velocity. The peak velocity amplitude is observed for the scenario when rupturing is towards the USC site (the same as in the previous case). For the scenario of the fault rupturing away from the USC site the synthetic seismograms are simple with very little late-arriving energy. However, seismograms due to both the bi-lateral and the

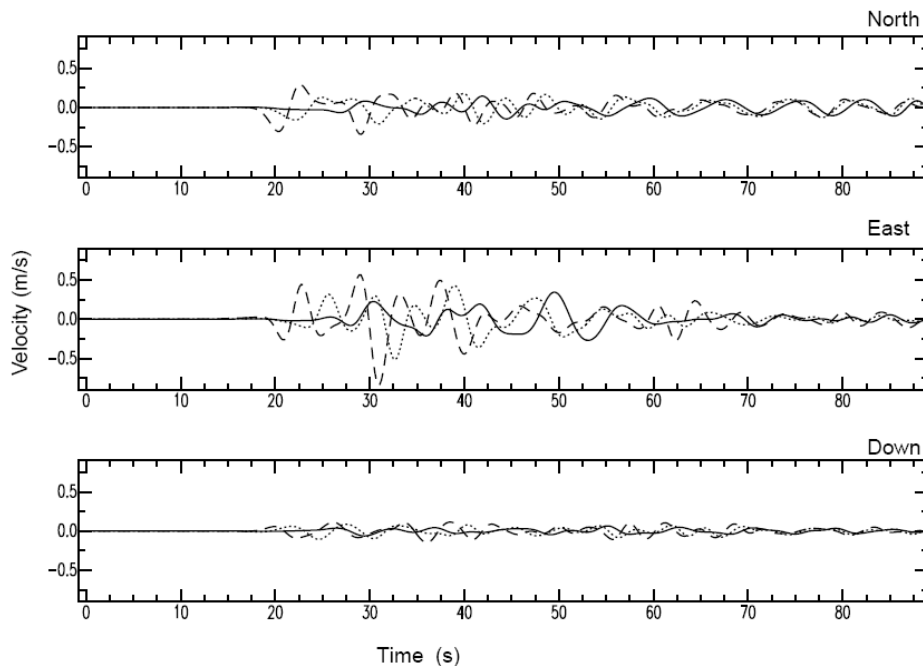


Fig. 3. Synthetic seismograms at the USC site for various fault rupturing scenarios of the Newport-Inglewood fault. All nine seismograms correspond to the earthquakes with rupture velocity equal to 90% of the S-wave velocity. The solid line represents a rupture scenario with a hypocenter at the center of the fault. The dotted line represents a rupture scenario with a hypocenter at the north-west edge of the fault at depth of 6.5 km. The dashed line is for the case with a hypocenter at the south-east edge of the fault at depth of 6.5 km.

unilateral rupture directed towards the USC site show significant late arrivals of scattered energy radiated towards the USC site.

The statistical comparison of the large number of synthetic seismograms is done for each site by measuring two characteristics of the synthetic seismograms: peak ground velocity and duration. The peak velocity is measured as the maximum amplitude of a vectorial sum of all 3 components over the entire seismogram. The duration is the time interval between the points at which 20% and 90% of the total energy has been recorded. This definition is similar to the definition of *Trifunac and Brady (1975)*, but we have shortened the interval to avoid biasing due to numerical dispersion.

Figs. 4–6 summarize the peak ground velocity amplitude comparison for the USC, SM and PAS sites. In almost all cases, the variation of peak ground velocity amplitudes due to the rupture scenario is at least a factor of three but in some cases it reaches factor of eight (the Newport-Inglewood fault at the USC or SM site). A factor of three in peak ground velocity amplitude variation is comparable or larger than the variations due to a only 3-D velocity structure (*Olsen and Archuleta, 1996*). The Newport-Inglewood fault produces the largest ground motions of all the cases tested.

Hypothetical earthquakes on the San Andreas and the Sierra Madre faults show similar peak ground velocity distribution at the USC site, despite the difference in distance of the faults from the site. There are three Sierra Madre fault earthquake scenarios with hypocenters at the center and the east end of the fault, which generate large peak ground velocity amplitudes at the SM site. This is probably caused by the efficient coupling of the earthquakes' directivity and the Los Angeles basin. A similar effect at the SM site can be observed for hypothetical earthquakes from the San Andreas fault for scenarios with the hypocenter at the south-east end of the fault. This observation emphasizes the importance of testing different rupture scenarios to evaluate realistic seismic hazard from a particular fault, because with the hypocenter at other locations on the fault, the peak velocities are 2–4 times smaller. Our peak ground velocity values are significantly smaller than those simulated by *Olsen and Archuleta (1996)* and are similar to the peak ground velocity values simulated by *Graves (1998)*. *Graves (1998)* gives a detailed analyses for the plausible reasons (uniform vs. non-uniform slip distribution, seismic moment to rupture area scaling) for this difference. The peak ground velocity amplitudes simulated for the Santa Susana fault at the USC and SM sites are similar to those observed for the Northridge Earthquake (*Olsen and Archuleta, 1996*). For the SM site the Newport-Inglewood fault is again the most hazardous fault. The large spread in the simulated peak ground velocity amplitudes at the SM site is due to earthquakes on the Newport-Inglewood fault, again emphasizing the importance of testing different rupture scenarios. The alternative source models discussed in the Appendix B would probably cause even stronger directivity effects and therefore a greater variation in the observed peak ground velocity amplitudes. The directivity effects would be caused by the smoother slip distribution (consistent superposition), and variation of the rise would certainly increase a variation observed seismograms. Therefore our results may underestimate the final variation of the peak ground velocity amplitudes.

The PAS site is located almost outside of the Los Angeles basin, and therefore, the peak velocities at the site are generally much smaller than the peak velocities for the SM and USC sites. The only large peak ground velocity amplitudes are observed for the

hypothetical earthquakes on the Sierra Madre. The large peak ground velocity amplitudes due to the earthquakes on the Sierra Madre fault are caused by the proximity of the fault to the site. Note that the peak velocity amplitude due an earthquake on the Sierra Madre fault varies by a factor of 3 for the PAS site.

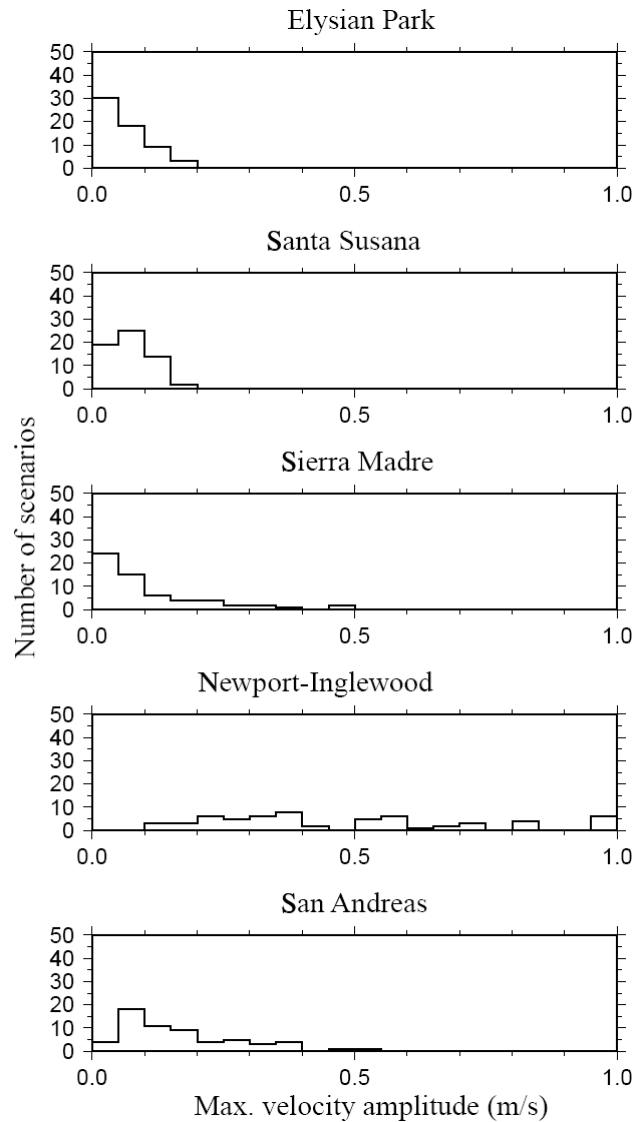


Fig. 4. Peak velocity amplitude of the velocity vector as recorded at the USC site from 60 different rupture scenarios: 3 different rupture velocities, 5 different hypocenters, and 4 different slip distributions for each fault.

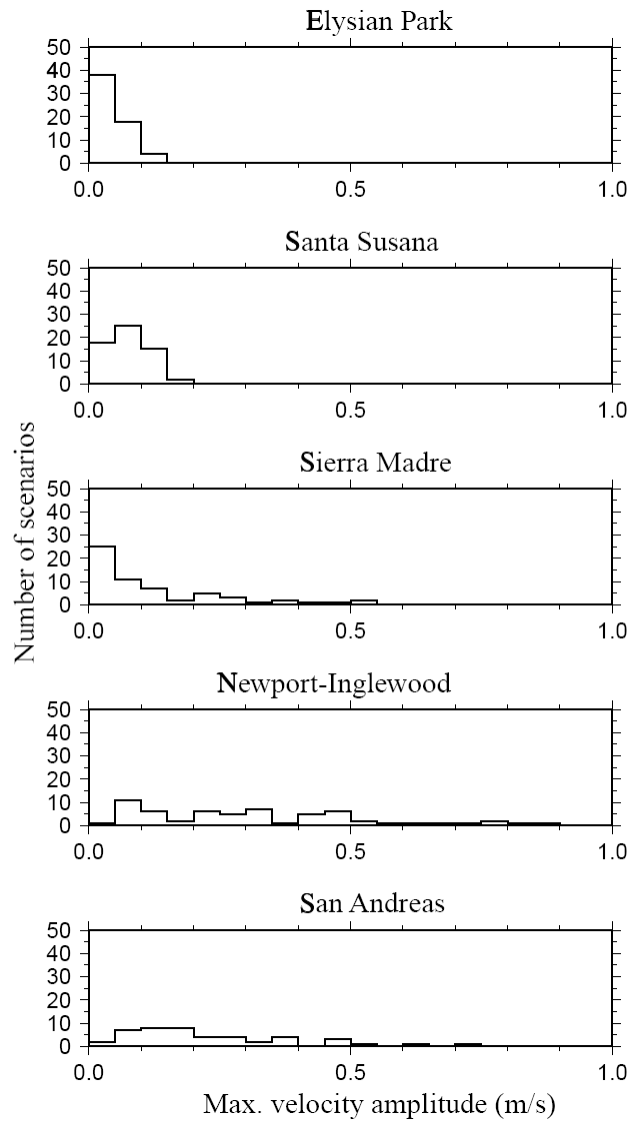


Fig. 5. Peak velocity amplitude of the velocity vector as recorded at the SM site from 60 different rupture scenarios: 3 different rupture velocities, 5 different hypocenters, and 4 different slip distributions for each fault.

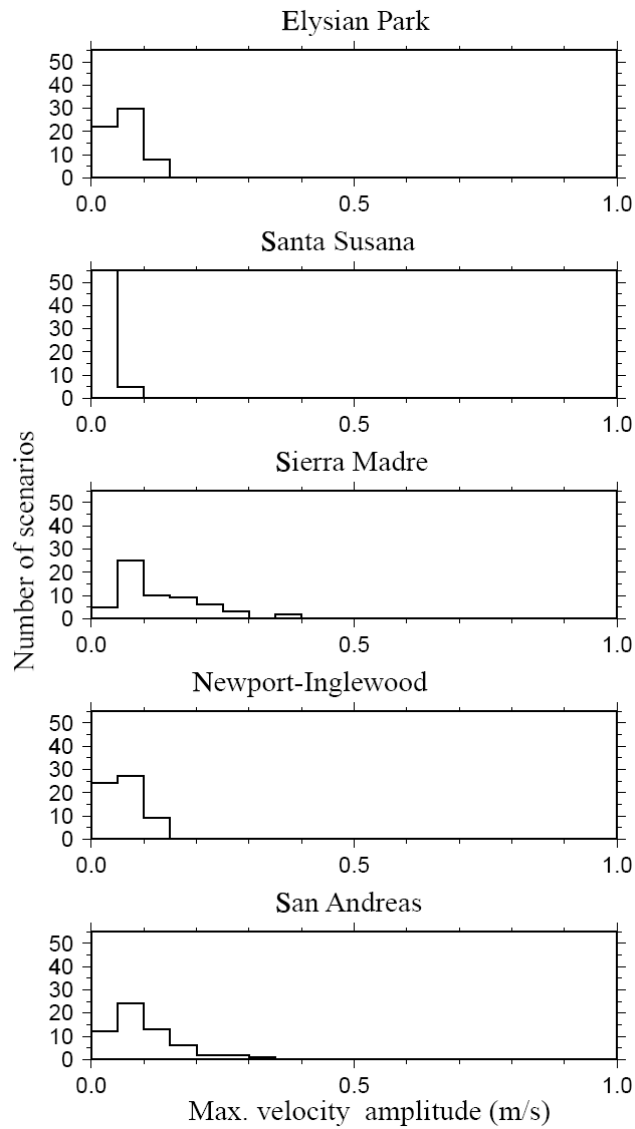


Fig. 6. Peak velocity amplitude of the velocity vector as recorded at the PAS site from 60 different rupture scenarios: 3 different rupture velocities, 5 different hypocenters, and 4 different slip distributions for each fault.

Fig. 7 summarizes the source durations (or slip duration on each fault) and site durations of the different rupture scenarios on the selected faults. Again, we can see that variation of parameters of the source rupture scenario may cause a factor of 2–4 variation in the duration at any site. The source durations increase with increasing size of the fault as the rupture velocity is limited by the shear wave velocity. The definition of the source durations is slightly different from the site durations. The source duration is defined as the time of the slip duration, e.i. the time between 0% and 100% of the released energy. Durations due to the San Andreas fault ruptures for the USC and SM sites are limited by the length of the computed seismograms (the first arrivals at USC and SM sites appear between 30–40 seconds after the rupture initiation).

The site durations are longer than the source durations for most of the rupture scenarios as the scattered energy in the heterogeneous velocity model tends to arrive later. Most of the durations at the SM site are two to three times as long as the source durations

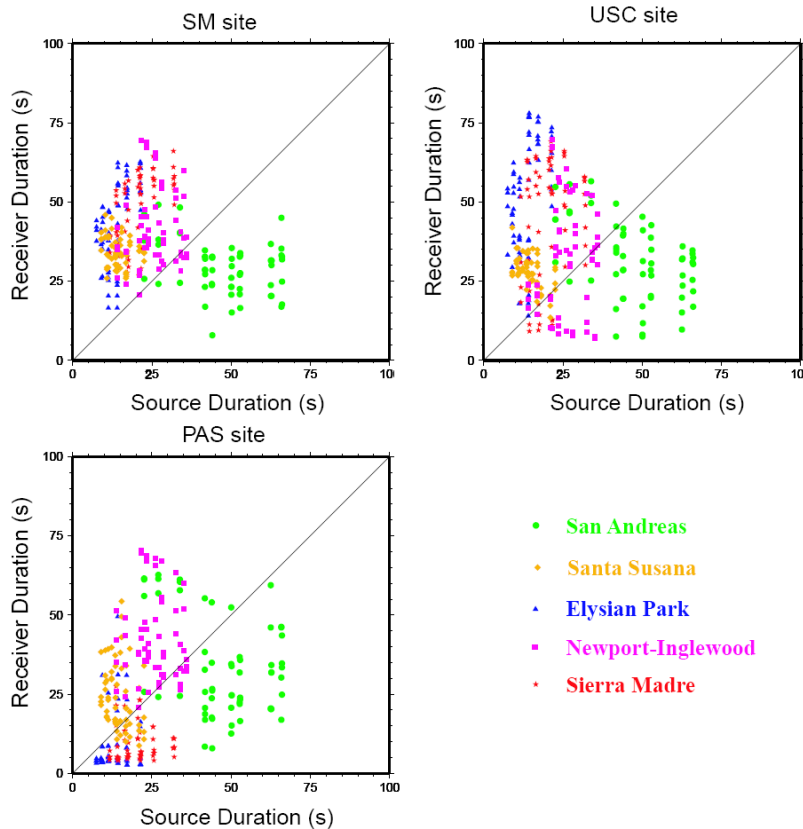


Fig. 7. The source and site durations for the selected site and 300 rupture scenarios. The source durations are measured from the initiation to the end of the rupture process, the site durations are measure as a time interval between 20 to 90% of energy in the seismogram.

for the Newport-Inglewood, Elysian Park and Santa Susana faults, because of the surface waves trapped in the sedimentary basins extend the durations at the SM sites. Similarly, most of the site durations at the USC site are two to three times as long as the source durations for the Newport-Inglewood, Elysian Park, and Santa Susana faults. The USC site's durations due to the earthquakes on the Newport-Inglewood fault show a significant dependence on the rupture scenarios; the scenarios in which the fault ruptures southward with a high velocity (90% of the S-wave velocity) have short durations. The durations due to the Elysian Park fault earthquakes show a strong dependency on the rupture scenarios at all sites; the ruptures with hypocenters at the south end of the fault show longer durations. The PAS site's durations due to earthquakes on the Newport-Inglewood, Elysian Park, and Santa Susana faults are strongly dependent on the rupture scenario, as only certain configurations tend to trap energy in the Los Angeles basin. The PAS site's durations due to the Sierra Madre fault earthquakes are relatively short as the PAS site is close to the fault in a weakly heterogeneous medium. However, strong heterogeneity significantly extends the duration of the signal as is shown by the PAS site's durations due to earthquakes on the Newport-Inglewood fault. Again the alternative source models discussed in the Appendix B may cause even stronger directivity effects and therefore a greater variation in the duration. However the variation of the rise would not increase a variation of the duration.

4. DISCUSSION AND DATA VALIDATION

The above presented results can be used for hazard assessment if they are consistent with previously observed data. The Southern California model was calibrated in a previous study (*Eisner and Clayton, 2002a*) by comparison of a large number of weak-motion earthquake recordings with synthetic seismograms. *Eisner and Clayton (2002a)* show that the misfit between the maximum amplitude of data and synthetics has a significant variation with azimuth, but the model does not generate a systematic bias. The strong-motion seismograms are evaluated by superposition of a time-staggered point source. The source models are discussed in the the Appendix B and we show that they are consistent with inverted source models of *Somerville et al. (1999)*. An alternative comparison with data can be done by simulating previously observed large earthquakes, this has been done by *Olsen and Archuleta (1996)* and *Wald and Graves (1998)* for two large earthquakes nearest to the Los Angeles basin. They have used the same finite difference techniques and similar models and were able to reproduce the observed data with even smaller misfit than that of *Eisner and Clayton (2002a)*. However, the two large earthquakes reproduce data in a 3-D model only from two directions not representative for the locations of the faults in our model. In fact validating a hazard assessment by fitting one or two large earthquakes would be like describing a 3-D object by looking at it from one or two views. Indeed, one needs at least three views to describe just a shape of a simple 3-D object not mentioning the interior of the object. As shown in this hazard assessment study the most important validation is by testing data with sources inside the Los Angeles basin. Finally, our results are consistent with the averaged peak ground velocity motion of *Campbell (1997)*. *Campbell (1997)* gives an average peak ground acceleration at distance 10 km from the fault to be approximately 0.1 meter per second

squared at 3 second period. Assuming a plane wave this translates to 5 cm/s peak ground velocity. Majority of our source scenarios give similar peak ground velocity, except the scenarios of a fault rupturing the deep part of the Los Angeles basin. *Campbell (1997)* did not include data from similar events as they were not available. This demonstrates the advantage of the proposed methodology which enables to evaluate realistic site-specific hazard assessment.

5. CONCLUSIONS

We have developed a method for evaluation of the site and path effects with full waveform synthetic seismograms that include a complex heterogeneous media and variable rupture scenarios. If the number of sites of interest is limited, the method reduces the required numerical simulations by a few orders of magnitude (33 times in this study). Using the Southern California Velocity Model we have evaluated the theoretical site effects for three locations in the Los Angeles area. The selected set of 300 rupture scenarios have shown that the variations due to rupture scenario on a fault causes a factor of 3–8 variation in the peak ground velocity amplitude for the selected sites, and a factor of 2–4 in the duration. We have found that the largest peak ground velocity amplitudes are observed from earthquakes on the nearest faults rather than from an earthquake on the San Andreas fault. The results presented here show that it is important to consider the complete set of faults in a region and the effects of wave propagation in hazard calculations.

APPENDIX A ATTENUATION ESTIMATE

Attenuation is not part of the Southern California Velocity Model. Here, we shall only estimate the attenuation effect on the peak velocity amplitude by a simple order of magnitude calculation. *Aki and Richards (1980, p. 168–9)* derive the attenuation effect in a homogeneous medium with an attenuation factor $Q(T) \gg 1.0$ for a wave with amplitude A_0 at point $x = 0$ and propagating with velocity c ; the amplitude of this wave at distance x is

$$A(x) = A_0 e^{-(\pi x/cTQ(T))}. \quad (\text{A1})$$

Using the engineering practice (c.f. *Kramer, 1996, Chapter 4*) we use the shortest distance from the finite fault from our site to estimate the distance x in Eq.(A1). Obviously, Eq.(A1) implies the longer the period of the propagating wave, the smaller the attenuation effects for a constant Q (not dependent on frequency). Therefore, we shall make our estimate only for the shortest period of 3 seconds. Eq.(A1) also implies that the faster propagating waves have smaller attenuation effects (at the same period and distance). To estimate an upper bound on the attenuation effects, we investigate surface waves, the slowest propagating waves at a given period.

It is difficult to estimate a representative crustal value of the attenuation at 3 seconds period $Q(3.0)$. The seismic waves are mainly attenuated at the very top of the crust (i.e. for high frequencies 90% of the signal is attenuated at the top 3 km of the crust (Abercrombie, 1997). However, there are very few measurements of attenuation at long periods for the strong motion data. *Su et al. (1988)* use a regional 1-D model of Southern California with values of $Q_S \sim 20-150$ (frequency-independent attenuation of the S-waves), which is consistent with value of $Q = 70$ found by *Hough (1997)* for frequencies 1–10 Hz at Ridgecrest, California, and $Q = 80-130$ from *Ma and Kanamori (1994)* for a frequency of approximately 1 Hz for the Sierra Madre earthquake, California. The representative values for sedimentary basins are in the lower range of the above values as can be seen in the *Ibanez et al. (1991)* study of attenuation in sedimentary basins. Therefore, we estimate the representative values for $Q(3.0) \sim 100$ for paths outside of sedimentary basins and $Q(3.0) \sim 50$ for paths inside sedimentary basins.

Assuming we can approximate the medium between the San Andreas fault and the PAS site by a homogeneous halfspace with $c = 3.0$ km/s (see Fig. 1) and a distance of $x \sim 50.0$ km, Eq.(A1) gives

$$\frac{A(50.0)}{A_0} < e^{(-17/Q(3.0))}.$$

This path is outside of the sedimentary basin and therefore the maximum amplitude is at most (we estimate the upper bound) reduced by 15% making the attenuation effect negligible. However, for a wave propagation inside the sedimentary basin we must be more careful. We can approximate the medium between the Newport-Inglewood fault and the PAS site as a homogeneous halfspace with $c = 0.7$ km/s (see Fig. 1) and a distance of $x \sim 30.0$ km. Eq.(A1) gives

$$\frac{A(30.0)}{A_0} < e^{(-45/Q(3.0))}.$$

This path is inside the Los Angeles sedimentary basin and therefore the maximum amplitude is at most reduced by 60% making the attenuation possibly more significant. However, this is an upper bound and therefore we know the maximum amplitudes without attenuation are a factor of 2 from the maximum amplitudes computed for models with a realistic attenuation. The effects of attenuation at the USC or SM sites are even smaller as the distances between faults and the sites are smaller. However, multiply scattered waves inside the basins may be more severely attenuated even at periods of 3 seconds. Therefore, our durations may be slightly overestimated and should be considered as an upper bound.

APPENDIX B SOURCE MODEL

For a single fault plane the kinematic model of an earthquake is determined by the slip distributions (both size and rake), the rupture velocity, the hypocenter location and the time history of rupture the each fault element (e.g. specified by the slip history of points on the fault).

The slip distributions (both size and rake) of the strike-slip Hector Mine, California, earthquake (*Ji et al., 2001*), the thrust-fault Chi Chi, Taiwan, earthquake (*Ma et al., 2001*), the thrust-fault Northridge, California, earthquake (*Wald et al., 1996*) and the strike-slip Landers, California, earthquake (*Wald and Heaton, 1994*) show that the slip size distribution on the fault plane are strongly heterogeneous. The slip rake orientation also varies around the average value. The inversions of the strong motion data prefer slip distribution concentrated in large asperities (e.g. *Wald et al., 1996; Ma et al., 2001*). In some cases, less than three asperities are required (Chi Chi, Northridge), but in others up to fifteen are needed (Landers, Hector Mine). To simulate realistic rupture scenarios, we have used four different slip distribution scenarios: two slip distribution models with only two large Gaussian asperities (with a peak slip that is ten times larger than the background slip) and two distributions with ten large Gaussian asperities (with a peak slip that is five times larger than the background slip). The definition of asperities in our model do not corresponds exactly to the asperities of *Somerville et al. (1999)* measuring average slip in an asperity (we characterize the asperity by a maximum slip) and counted small connected asperities as a single asperity. If similar definitions would be used the two large asperities model would have 3–4 times larger amplitudes and the ten asperities would model would reduce to 3–4 asperities with average slip 2–3 times larger than background, hence our slip models are consistent with *Somerville et al. (1999)*. All asperities are located in a Monte Carlo fashion on the fault surface. Fig. 8 shows four slip distributions used for a simulations of rupture on the San Andreas fault. The strike and dip of each point on the fault is determined by the fault's orientation. We randomized the slip's rake orientation within a maximum of 20 degrees from the average rake on the fault. The randomized slip moment was smoothed over a distance of 5 km and renormalized to keep the total scalar moment M_0 the same.

The rupture velocity is an important parameter of the rupture scenario which can not be entirely predicted. We have set the rupture speed relative to a constant fraction of the local shear-wave speed (*Olsen and Archuleta, 1996; Aagaard et al., 2001*). To compute the rupture front time history, we use a simplified 2-D finite-difference travel-time algorithm (*Vidale, 1988*). To account for an unknown ratio of the rupture velocity to the S-wave velocity on the fault, we tested several values of the rupture velocity: 60%, 75%, and 90% of the S-wave velocity on the fault.

Hypocenter location is another unknown variable of the rupture scenario. We tested 5 different locations of the hypocenter on the fault: one in the center of the fault (representing bi-lateral scenario) and two locations on each side of the fault - one at the bottom of the fault and one at the center of the side of the fault.

We have not varied the slip history (set to a ramp with the 3 seconds length) of each point on the fault. An alternative slip history functions can be accounted for by

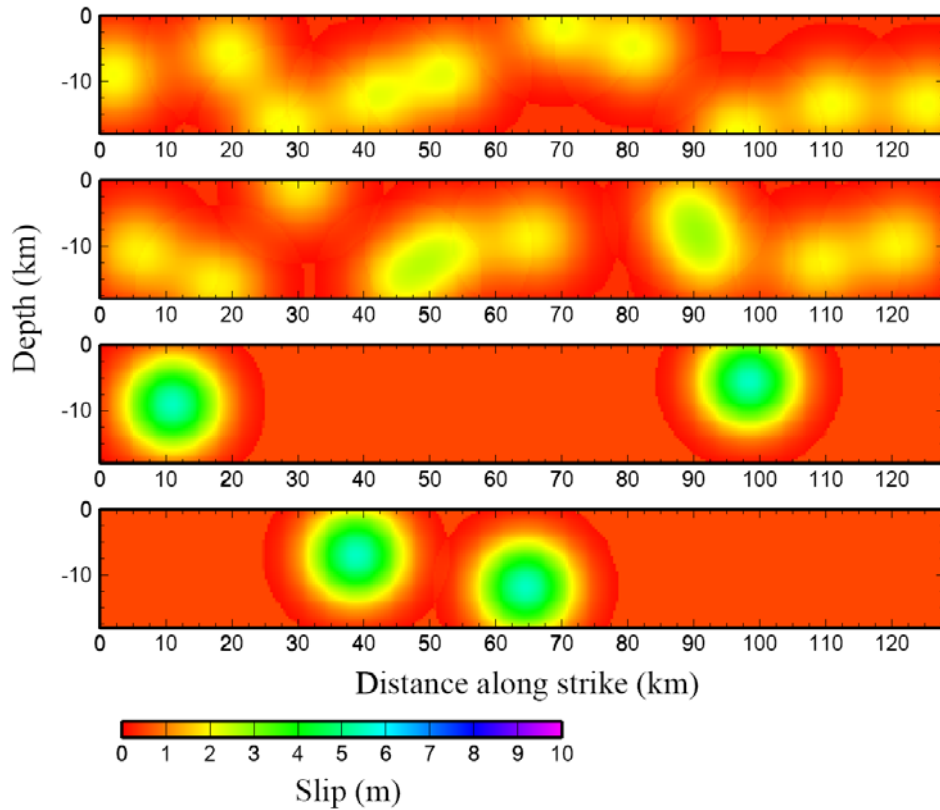


Fig. 8. Four scenarios of a slip distribution on the San Andreas fault. The slip distribution is forced into randomly located asperities. The net moment is the same for all models.

deconvolving the slip history function used in the simulation from the seismograms and re-convolving with the alternative slip history function. The slip history function does not influence the effects due to dynamic of the rupture or wave-propagation in a heterogeneous medium. Also, variation in the slip history does not appear to be a significant factor for the period range of interest in this study. For example, *Aagaard et al. (2001)* did not observe significant effects on the strong motion seismograms due to a realistic variation of the slip history. The slip history does, however, play an important role for shorter period seismic wave propagation and its variability should be factored into site and path effect for these periods.

We have also not considered smoother slip distributions or rescaling a slip distribution of an earthquake to the size of fault planes of interest (e.g. *Graves, 1998*). The smoother slip distributions may result from smoothed inversion procedures. We do not know how to correctly randomize the rescaling of a slip distribution of an earthquake. However we tested a large number of slip distributions and the conclusions of this paper are not affected by these alternative slip distributions. We have also not tested the possibility of

the super-shear velocity rupture (e.g. *Bouchon et al., 2001*). As it is discussed in the main text most of the alternative source scenarios should only strengthen our conclusions. It is not an aim of this article to use all possible source scenarios, however the reciprocity method can evaluate response due to slip distribution and it is possible to use it for further studies of the source effects.

Acknowledgments: The authors would like to thank Hiroo Kanamori, Tom Heaton, Ned Field, Jifi Zahradnik and three anonymous reviewers and the associate editor for their valuable suggestions and discussion during the study. Many of the figures were made with GMT (*Wessel and Smith, 1991*). This research was supported by the Southern California Earthquake Center. SCEC is funded by NSF Cooperative Agreement EAR-8920136 and USGS Cooperative Agreements 14-08-0001-A0899 and 1434-HQ-97AG01718. The SCEC contribution number for this paper is 558. Contribution number 8821 from the Division of Geological and Planetary Sciences, California Institute of Technology.

References

- Aagaard B., Hall J., Heaton T. and Eeri M., 2001. Characterization of near-source ground motions with earthquake simulations *Earthquake Spectra*, **17**, 177–207.
- Abercrombie R., 1997. Near-surface attenuation and site effects from comparison of surface and deep borehole recordings. *Bull. Seismol. Soc. Amer.*, **87**, 731–744.
- Aki K. and Richards P., 1980. *Quantitative Seismology*. W.H. Freeman and Co., San Francisco, USA.
- Bouchon M., Boulin M.-P., Karabulut H., Toksöz M., Dietrich M. and Rosakis A., 2001. How fast is rupture during an earthquake? new insights from the 1999 Turkey earthquakes. *Geophys. Res. Lett.*, **28**, 2723–2726.
- Campbell K., 1997. Empirical near-source attenuation relationships for horizontal and vertical components of peak ground acceleration, peak ground velocity, and pseudo-absolute acceleration response spectra. *Seism. Res. Lett.*, **68**, 154–179.
- Eisner L. and Clayton R.W., 2001. A reciprocity method for multiple source simulations. *Bull. Seismol. Soc. Amer.*, **91**, 553–560.
- Eisner L. and Clayton R.W., 2002a. A full waveform test of the southern California velocity model by the reciprocity method. *Pure Appl. Geophys.*, **159**, 1691–1706.
- Eisner L. and Clayton R.W., 2002b. Equivalent medium parameters for numerical modelling in media with near-surface low-velocities. *Bull. Seismol. Soc. Amer.*, **92**, 711–722.
- Field E. and the SCEC Phase III Working Group, 2000. Accounting for site effects in probabilistic seismic hazard analyses of Southern California: Overview of the SCEC Phase III report. *Bull. Seismol. Soc. Amer.*, **90**, S1–S31.
- Graves R., 1996. Simulating seismic wave propagation in 3D elastic media using staggered-grid finite differences. *Bull. Seismol. Soc. Amer.*, **86**, 1091–1106.
- Graves R., 1998. Three-Dimensional finite-difference modeling of the San Andreas fault: Source parameterization and ground-motion levels. *Bull. Seismol. Soc. Amer.*, **88**, 881–897.

Simulating Strong Ground Motion from Complex Sources by Reciprocal Green Functions

- Graves R. and Wald D., 2001. Resolution analysis of finite fault source inversion using 1D and 3D Green's functions, part I: Strong motions. *J. Geophys. Res.*, **106**, 8745–8766.
- Hough S., 1997. Empirical Green's function analysis: Taking the next step. *J. Geophys. Res.*, **102**, 5369–5384.
- Ibanez J., Morales J., DeMiguel F., Vidal F., Alguacil G. and Posadas A., 1991. Effect of a sedimentary basin on estimations of q_c and q_{Lg} . *Phys. Earth Planet. Inter.*, **66**, 244–252.
- Ji C., Wald D. and Helmberger D., 2001. Source description of the 1999 Hector Mine, California, earthquake; Part II: Complexity of slip history. *Bull. Seismol. Soc. Amer.*, **92**, 1208–1226.
- Kramer S., 1996. *Geotechnical Earthquake Engineering*. Prentice-Hall, Inc., Upper Saddle River, NJ, USA.
- Liu P. and Archuleta R., 2000. A preliminary finite fault inversion of the 1999 M7.7 Chi Chi, Taiwan earthquake using 3-d Greens functions. *EOS AGU Trans.*, **81**, F874.
- Ma K., Mori J., Lee S. and Yu S., 2001. Spatial and temporal distribution of slip for the 1999 Chichi, Taiwan, earthquake. *Bull. Seismol. Soc. Amer.*, **91**, 1069–1087.
- Ma K.-F. and Kanamori H., 1994. Broadband waveform observation of the 28 June 1991 Sierra-Madre earthquake sequence ($M(l) = 5.8$). *Bull. Seismol. Soc. Amer.*, **84**, 1725–1738.
- Magistrale H., Day S., Clayton R. and Graves R., 2000. The SCEC Southern California Reference 3D Seismic Velocity Model Version 2. *Bull. Seismol. Soc. Amer.*, **90**, S65–S76.
- Olsen K., 2000. Site amplification in the Los Angeles basin from three-dimensional modeling of ground motion. *Bull. Seismol. Soc. Amer.*, **90**, 677–685.
- Olsen K. and Archuleta R., 1996. Three-dimensional simulation of earthquakes on the Los Angeles fault system. *Bull. Seismol. Soc. Amer.*, **86**, 575–596.
- Petersen M., Bryant W., Cramer C., Cao T., Riechle M., Frankel A., Lienkaemper J., McCrory P. and Schwartz D., 1996. *Probabilistic Seismic Hazard Assessment for the State of California*. Technical Report, Division of Mines and Geology, open-file report 96-08; United States Geological Survey; open-file report 96-706.
- Somerville P., Irikura K., Graves R., Sawada S., Wald D., Abrahamson N., Iwasaki Y., Kagawa T., Smith N. and Kowada A., 1999. Characterizing crustal earthquake slip models for the prediction of strong ground motion. *Seism. Res. Lett.*, **70**, 59–80.
- Spudich P., 1981. Frequency domain calculation of extended source seismograms. *EOS Trans. AGU*, **62**, 960.
- Su F., Anderson J. and Zeng Y., 1988. Study of weak and strong ground motion including nonlinearity from the Northridge, California, earthquake sequence. *Bull. Seismol. Soc. Amer.*, **88**, 1411–1425.
- Trifunac M. and Brady A.G., 1975. A study of the duration of strong ground earthquake ground motion. *Bull. Seismol. Soc. Amer.* **65**, 581–626.
- Vidale J., 1988. Finite-difference calculation of travel-times. *Bull. Seismol. Soc. Amer.*, **78**, 2062–2076.
- Wald D. and Graves R., 1998. The seismic response of the Los Angeles basin, California. *Bull. Seismol. Soc. Amer.*, **88**, 337–356.
- Wald D. and Heaton T., 1994. Spatial and temporal distribution of slip for the 1992 Landers, California, earthquake. *Bull. Seismol. Soc. Amer.*, **84**, 668–691.

- Wald D., Heaton T. and Hudnut K., 1996. The slip history of the 1994 Northridge, California, earthquake determined from strong-motion, teleseismic, GPS, and leveling data. *Bull. Seismol. Soc. Amer.*, **86**, S49–S70.
- Wells D. and Coppersmith K., 1994. New empirical relationships among magnitude, rupture length, rupture width, rupture area, and surface displacement. *Bull. Seismol. Soc. Amer.*, **84**, 974–1002.
- Wessel P. and Smith W., 1991. Free software helps map and display data. *EOS Trans. AGU*, **72**, 441.